ACS Sustainable Chemistry & Engineering

Research Article

Cite This: ACS Sustainable Chem. Eng. 2018, 6, 12471−12480

pubs.acs.org/journal/ascecg

Enhanced Electromagnetic Wave Absorption of Three-Dimensional Porous Fe_3O_4/C Composite Flowers

Nannan Wu,[†,§] Chang Liu,[†] Dongmei Xu,[‡] Jiurong Liu,*[,†] Wei Liu,[‡] Qian Shao,[∥] and Zhanhu Guo[§]

[†]Key Laboratory for Liquid−Solid Structural Evolution and Processing of Materials, Ministry of Education and College of Materials Science and Engineering, Shandong University, No. 17923 Jingshi Road, Lixia District, Jinan, Shandong 250061, China

[‡]State Key Laboratory of Crystal Materials, Shandong University, No. 27 Shanda South Road, Jinan, Shandong 250100, China

[§]Integrated Composites Laboratory (ICL), Department of Chemical & Biomolecular Engineering, University of Tennessee, 1512 Middle Drive, Knoxville, Tennessee 37996, United States

[∥]College of Chemical and Environmental Engineering, Shandong University of Science and Technology, 579 Qianwangang Road, Huangdao District, Qingdao, Shandong 266590, China

ABSTRACT: Magnetite (Fe_3O_4)/carbon (C) composite flowers with an average size of 4−6 μm were prepared through a facile route including a solvothermal approach and a carbon reduction process. The resultant Fe_3O_4/C composites are porous and exhibit a three-dimensional (3D) flower-like morphology with the core−shell Fe_3O_4@C nanoparticles hybridized by amorphous carbon sheets. The epoxy resin composites containing 50 wt % 3D porous Fe_3O_4/C composite flowers display an optimal reflection loss (RL) value of −54.6 dB at 5.7 GHz at a thin thickness of 4.27 mm and the effective bandwidth with RL < −10 dB reaches 6.0 GHz at a thickness of 2.1 mm. These enhanced EM wave absorption performances are attributed to the synergistic effects of Fe_3O_4 and carbon as well as the structural advantages, e.g., three-dimensional structure with large surface area, porous and core−shell structures of Fe_3O_4/C flowers. These results suggest the 3D porous Fe_3O_4/C composite flowers designed here can serve as ideal candidates for high-performance EM wave absorption.

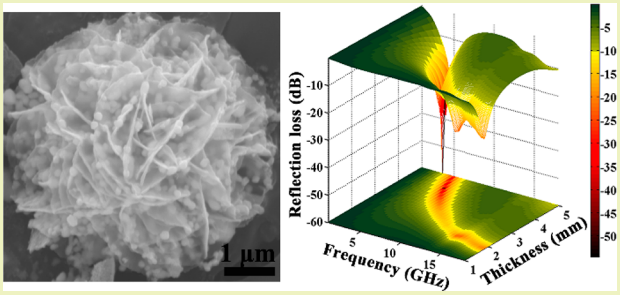

KEYWORDS: *Electromagnetic wave absorption, Composite, Magnetite, Carbon, Three-dimensional*

INTRODUCTION

Nowadays, tremendous efforts have been devoted to the fabrication of electromagnetic (EM) wave absorption materials in order to solve the increasingly electromagnetic radiation pollution arising from the rapid development of electronic devices.[1−6] As an important kind of magnetic material, Fe_3O_4 has drawn a great deal of attentions because of its low cost and unique magnetic features, such as a proper saturation magnetization value and high Curie temperature, thus providing great potential to be applied as high-efficiency EM wave absorbers.[7−11] However, pure Fe_3O_4 absorbers always suffer from a lot of drawbacks such as a dramatic decrease of permeability in high frequency range due to the Snoek's limit, ease of oxidation, and high density, which is unable to satisfy the requirements of an ideal EM absorber with strong absorption ability, broad absorption bandwidth, thin absorber thickness and low density. One effective way to overcome these problems is to design core−shell structured composites with Fe_3O_4 as the core and a dielectric shell. Among a variety of dielectric materials, carbon materials especially at the nanoscale, for their lightweight, abundant resources, large aspect ratio and good conductivity, are always the most attractive candidates to improve EM wave absorption performances.[12−15] These core−shell Fe_3O_4/C composites were found not only to significantly improve the impedance matching due to the synergy effect of strong magnetic loss from magnetite cores and dielectric loss from carbon shells but also to effectively reduce the density of the absorbers and protect the magnetite core from environmental oxidation, giving rise to enhanced EM wave absorption properties than their individual components. For example, Du et al. demonstrated a successful preparation of core−shell Fe_3O_4/C microspheres with different shell thicknesses and the microwave absorption properties were investigated.[15] The reflection loss (RL) lower than −10 dB (90% absorption) was achieved from 4.0 to 18 GHz with a thickness range of 1.5−5.0 mm. Chen et al. have synthesized porous Fe_3O_4/C core−shell nanorods via a three-step process and the minimum RL reached −27.9 dB at 14.96 GHz attributing to their improved impedance matching.[16]

Apart from constructing core−shell structured composites, fabricating materials with flake structure has been another effective way to obtain high-efficiency EM absorbers. Large

Received: June 30, 2018
Revised: July 27, 2018
Published: August 2, 2018

DOI: 10.1021/acssuschemeng.8b03097
ACS Sustainable Chem. Eng. 2018, 6, 12471−12480

shape anisotropy of flake-shaped structure can exceed the traditional Snoek's limit, leading to a larger permeability in GHz range.[17−19] Recently, the 3D flower-like structure assembled by abundant flakes has been promising for EM wave absorption, such as flower-like FeNi@C nanocomposites with an optimal RL of −47.6 dB at 3.17 GH.[20] Lv et al. have prepared porous 3D flower-like Co/CoO with an optimal RL value of −50 dB at 7.2 GHz, and the bandwidth was up to 4.2 GHz at a thickness of 2.0 mm.[18] The excellent EM absorption is associated with a better impedance matching between permeability and permittivity of the composites. Moreover, special 3D flower-like structure of Co/CoO composites with the presence of pores can cause multiple scattering and reflection, which contribute to the dissipation of incident EM waves as well. However, there are few studies concerning about the synthesis and applications of 3D flower-like structured Fe_3O_4 as EM absorbers. Li et al.[21] have synthesized the porous Fe_3O_4 flower-like nanostructures successfully, but the optimal RL value was only −28.31 dB and the effective absorption bandwidth (RL < −10 dB) was 3.8 GHz, which also needed to be broadened.

In this study, porous Fe_3O_4/C composite flowers were prepared via solvothermal method followed by a carbon reduction process. These composite flowers exhibit a three-dimensional flower-like shape that was composed of core−shell Fe_3O_4/C nanoparticles coated with amorphous carbon sheets. The microstructures and compositions of the porous Fe_3O_4/C composite flowers were studied by X-ray diffraction (XRD), field emission scanning electron microscopy (FE-SEM), transmission electron microscope (TEM). The carbon content in the porous Fe_3O_4/C composite flowers was evaluated by thermogravimetric analysis. The EM parameters including complex permittivity and complex permeability were measured from 1.0 to 18.0 GHz. The resultant 3D porous Fe_3O_4/C composite flowers present an enhanced EM wave absorption performance comparing with previously reported pure Fe_3O_4 and other Fe_3O_4/C composites and the mechanisms for the enhanced EMI shielding were clarified in terms of synergistic effects between Fe_3O_4 and carbon as well as the structural features.

EXPERIMENTAL SECTION

Materials. Ferric chloride ($FeCl_3·6H_2O$), urea, ethylene glycol and pyrrole were obtained from Sinopharm Chemical Reagent Co., Ltd. All chemicals were analytical grade and used without further purification.

Preparation of 3D Porous Fe_3O_4/C Composite Flowers. The 3D porous Fe_3O_4/C composite flowers were prepared by adopting a two-step strategy including a facile synthesis of Fe_2O_3 flowers as an intermediate and a following carbon reduction process by using pyrrole as carbon source. In a typical procedure, 0.5 mmol ferric chloride and 3.0 mmol urea were dissolved in 25 mL of ethylene glycol, and the solution was constantly stirred for 1 h at room temperature. Subsequently, the formed homogeneous solution was transferred into a Teflon-lined stainless-steel autoclave (60 mL capacity), which was maintained at 160 °C for 10 h and then allowed to cool down to room temperature. After reaction, the yellow precursor was collected by centrifugal separation, then washed with deionized water for several times and finally dried in a vacuum oven at 60 °C for overnight. The Fe_2O_3 intermediate was obtained by calcinating the as-synthesized precursors in air at 400 °C for 1 h. The final product was obtained through a carbon reduction process by mixing 1 g of as-obtained Fe_2O_3 powders and 0.5 mL of pyrrole in a sealed steel autoclave and heated at 550 °C for 5 h.

Preparation of Samples for Electromagnetic Measurements. In order to investigate the EM properties of the as-synthesized 3D porous Fe_3O_4/C composite flowers, the samples were fabricated by homogeneously dispersing the products into epoxy resin with mass ratio of 50 wt %. Then the Fe_3O_4/C-epoxy resin composites were cut into a toroidal-shaped specimen with an outer diameter of 7.00 mm and an inner diameter of 3.04 mm for EM measurements.

CHARACTERIZATIONS

The compositions and crystal structures of the Fe_3O_4/C composite flowers were characterized by X-ray diffraction (XRD) instrument with Cu K radiation (λ = 0.154 06 nm) at 40 mA and 40 kV ranging from 10° to 80°. The surface morphology of the products and distribution of the elements were observed by a field emission scanning electron microscopy (FE-SEM, JSM-6700F) equipped with an energy dispersive spectrometer (XFlash 5030, Bruker, Germany). The microstructure of the 3D porous Fe_3O_4/C composite flowers was analyzed by a JEOL JEM-2100 transmission electron microscopy (TEM) operating at an accelerating voltage of 200 kV. In order to evaluate the carbon content in Fe_3O_4/C composites, thermogravimetric analysis was carried out on a SDT Q600 analyzer from room temperature to 800 °C at a heating rate of 10 °C min^{-1}. Nitrogen adsorption−desorption isotherms were recorded at 77 K on a QUADRASORB SI-KR/MP (Quantachrome, USA) instrument. The magnetic properties of the products were studied by a vibrating sample magnetometer (VSM, Lake Shore 7400) at room temperature. A network analyzer (Agilent Technologies N5244A) was applied to test the complex permeability (μ_r) and complex permittivity (ε_r) of the as-prepared toroidal samples using the coaxial-line method in frequency range of 1−18 GHz.

RESULTS AND DISCUSSION

Scheme 1 presents the synthesis procedures of 3D porous Fe_3O_4/C composite flowers. First, Fe_2O_3 flowers were obtained via a solvothermal reaction and a following calcination treatment in air. Then, 3D porous Fe_3O_4/C composite flowers were produced after the carbon reduction process by using pyrrole as the carbon source. During this process, carbon was connected together to form carbon sheets and the reduced Fe_3O_4 particles grew at the carbon sheets gradually with increasing the temperature. Hence, pyrrole played two roles in the formation of 3D porous Fe_3O_4/C composite flowers. On one hand, it acted as the reductant. Carbon was generated from the pyrolysis of pyrrole with increasing the temperature to 550 °C and reduced Fe_2O_3 to Fe_3O_4, during which a carbon shell was coated on Fe_3O_4

Scheme 1. Schematic Illustration of the Synthesis Procedure for 3D Porous Fe_3O_4/C Composite Flowers

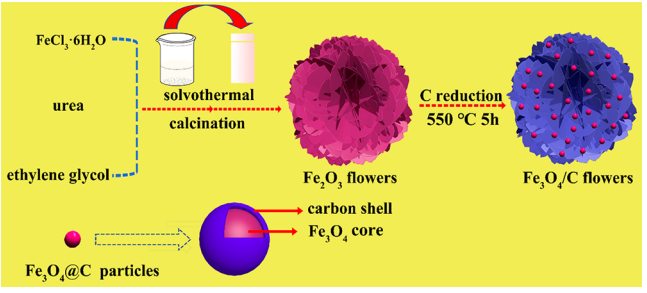

DOI: 10.1021/acssuschemeng.8b03097
ACS Sustainable Chem. Eng. 2018, 6, 12471−12480

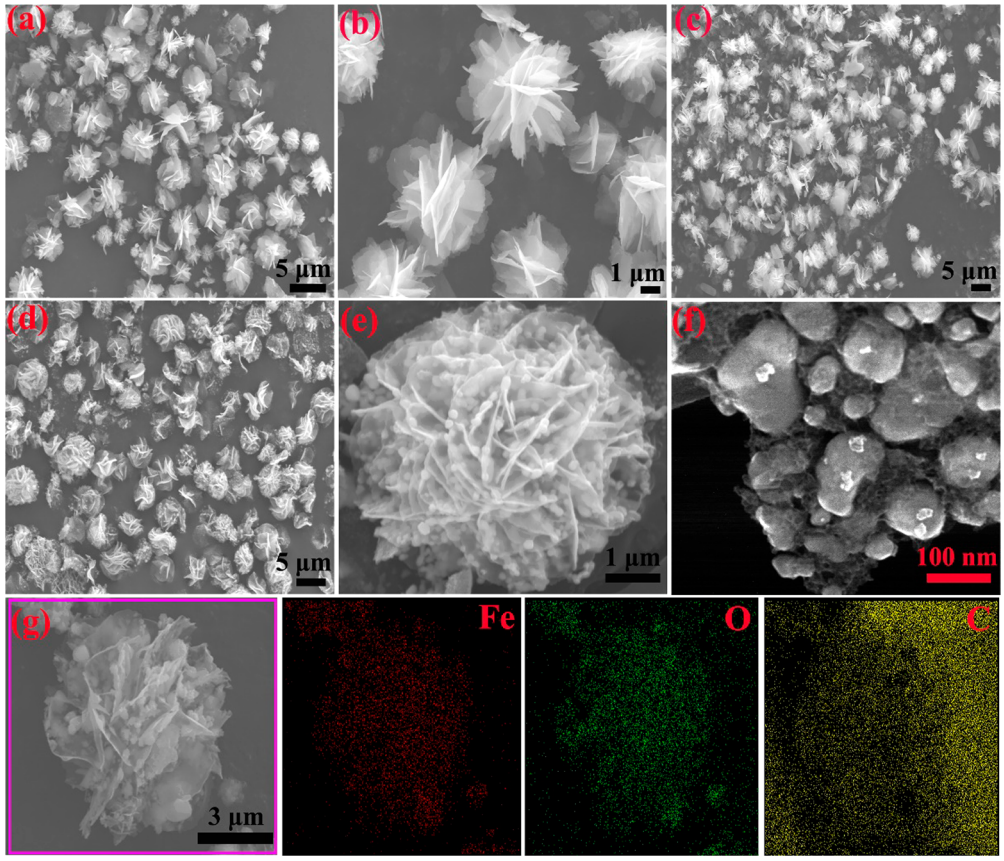

Figure 1. SEM images of the as-synthesized precursor (a and b), Fe_2O_3 flowers (c), 3D porous Fe_3O_4/C composite flowers (d and e), (f) petal surfaces for 3D porous Fe_3O_4/C composite flowers; (g) elemental mappings of 3D porous Fe_3O_4/C composite flowers.

particles. On the other hand, it served as a carbon source for the carbon deposition to form carbon sheets.

Figure 1a,b reveals the morphology of the precursor after the solvothermal reaction. As observed in Figure 1a, the precursor displays a monodisperse 3D flower-like morphology with an average size of 4−6 μm. The precursor is observed to be self-assembled by numerous smooth ultrathin petals as shown in the amplified image, Figure 1b. After calcination treatment in air, no apparent variations can be detected in the shape of Fe_2O_3 flowers (Figure 1c). Figure 1d exhibits the SEM images of 3D porous Fe_3O_4/C composite flowers. No obvious distinctions were observed in the overall size for Fe_3O_4/C flowers but with a great number of particles dispersed on the petal surface, and the dispersed particle sizes display a quite nonuniform distribution from tens of nanometers to hundreds of nanometers since the grain size can be greatly influenced by the heat treatment or solution temperature.[22,23] An individual Fe_3O_4/C flower was composed of two-dimensional flakes and numerous particles observing from the amplified image in Figure 1e. Taking a closer observation at the petal surfaces of 3D porous Fe_3O_4/C composite flowers in Figure 1f, the particle sizes vary between 20 and 150 nm. In addition, a lot of pores and defects were present on the sheets. To illustrate the spatial distribution of Fe, O and C, the elemental mapping was carried out on an individual Fe_3O_4/C flower, Figure 1g. The obtained results demonstrate that the Fe_3O_4 particles spread all over the structures and display a highly homogeneous dispersion with the presence of carbon.

Figure 2a shows the XRD patterns of the as-synthesized precursor, Fe_2O_3 flowers and 3D porous Fe_3O_4/C composite

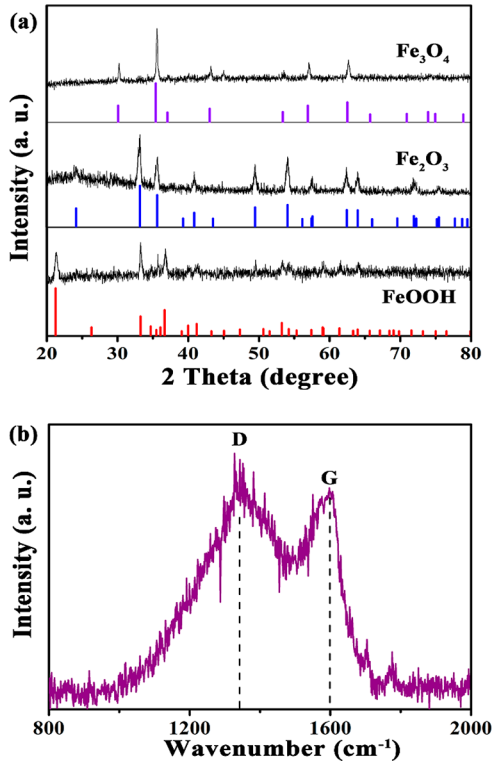

Figure 2. (a) XRD patterns of the as-synthesized precursor, Fe_2O_3 intermediate and 3D porous Fe_3O_4/C composite flowers and (b) Raman spectrum of the Fe_3O_4/C composite flowers.

DOI: 10.1021/acssuschemeng.8b03097
ACS Sustainable Chem. Eng. 2018, 6, 12471−12480

flowers. The diffraction peaks of the precursor can be assigned to FeOOH (JCPDS No. 29-0713). After the calcination, the diffraction peaks at 24°, 33°, 36°, 49°, 54°, 62° and 64° corresponding to Fe_2O_3 intermediate (JCPDS No. 80-2377) can be clearly seen, indicating the conversion of FeOOH to Fe_2O_3 during the heat treatment. When reduced by carbon, all diffraction peaks at 30°, 35°, 57° and 62°can be typically indexed to Fe_3O_4 (JCPDS Card No. 19-0629), suggesting the complete reduction of Fe_2O_3 to Fe_3O_4. By using the Scherrer equation, the average grain size of the Fe_3O_4 particles is calculated to be 95.6 nm. No other diffraction peaks have been detected, implying the Fe_3O_4/C flowers are almost without oxidation due to the protection of carbon shell. In addition, no diffraction peaks of carbon were observed in the XRD pattern, indicating that the carbon may exist mainly in an amorphous state. The information about the structure of carbon in the Fe_3O_4/C composite flowers is further investigated by Raman analysis (Figure 2b). Two characteristic peaks centered at ca. 1340 and 1595 cm^{-1} were observed, which respectively correspond to the D band representing amorphous carbon and the G band originating from graphite carbon.[7] Thus, the intensity ratio between D band and G band (I_D/I_G) can be used to evaluate the graphitization degree. The I_D/I_G value for the Fe_3O_4/C composite flowers is calculated to be 1.16. demonstrating a low graphitization degree, which is in accordance with the XRD results.

The detailed structure is further confirmed by TEM observations (Figure 3a–d). The Fe_3O_4/C composite flowers

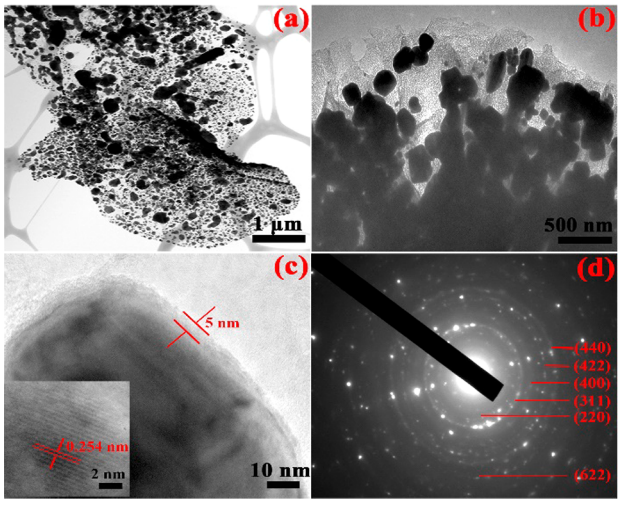

Figure 3. (a, b) TEM, (c) HR-TEM images and (d) SAED patterns of 3D porous Fe_3O_4/C composite flowers. The inset is the lattice spacing taken from the particles in Figure 3c.

are observed to be constructed by two-dimensional sheets and numerous particles with the size in the range of 20–300 nm (Figure 3a). In Figure 3b, the two-dimensional sheets are confirmed to be amorphous carbon sheets, which is in accordance with the XRD results. Obviously, the carbon sheets display a porous characteristic, Figure 3b, attributing to the release of carbon oxides during the high temperature carbon reduction process.[24] To further confirm the structure and compositions of Fe_3O_4/C flowers, the HR-TEM image of an individual particle is shown in Figure 3c. On one hand, the interplanar spacing of 0.254 nm can be assigned to the (311) plane of magnetite (the inset Figure 3c), indicating the formation of Fe_3O_4 core. On the other hand, a carbon layer of ca. 5 nm distributing around Fe_3O_4 particles can be detected, indicating a core–shell structure. The selected-area electron diffraction (SAED) pattern of 3D porous Fe_3O_4/C composite flowers is shown in Figure 3d. The diffraction rings can be well assigned to the (220), (311), (400), (422), (440) and (622) planes of Fe_3O_4,[8] which is in accordance with XRD results, further confirming the successful synthesis of 3D porous Fe_3O_4/C composite flowers.

To evaluate the weight percentage of carbon in the 3D porous Fe_3O_4/C composite flowers, TGA measurement was conducted in air from room temperature to 800 °C. As shown in Figure 4, the weight loss of ca. 1.1% observed below 150 °C

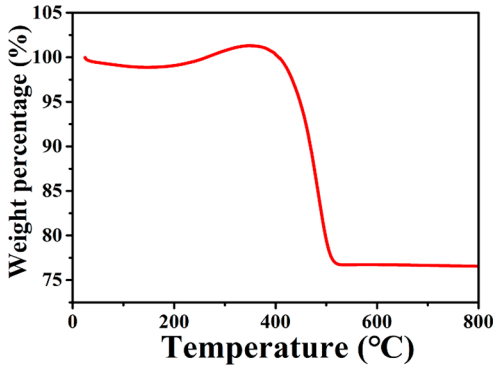

Figure 4. TGA curves of the 3D porous Fe_3O_4/C composite flowers measured in air from room temperature to 800 °C.

is ascribed to the evaporation of water.An intense weight lose of 22.1% occurred in the temperature range of 150–500 °C indicates a simultaneous process of the combustion of carbon and oxidation of Fe_3O_4 to Fe_2O_3. As carbon can be oxidized completely in air at 800 °C, the total 76.8% weight (100%–1.1%–22.1%) should only be the left Fe_2O_3. Based on the above analysis, the content of carbon in the 3D porous Fe_3O_4/C composite flowers can be calculated by Equation 1:

$$wt\%_L = \frac{3(1 - wt\%_{carbon} - wt\%_{water})}{2M_{Fe_3O_4}} \times M_{Fe_2O_3} \quad (1)$$

where wt $\%_L$ is the weight percentage of left Fe_2O_3, and M represents molecular weight of the chemicals. The weight ratio of carbon in the porous Fe_3O_4/C composite flowers is calculated to be ca. 24.6 wt %, and Fe_3O_4 content is about 76.4 wt %.

Porous structures involving low density and high specific surface areas are found to be beneficial for improving the EM wave absorption performances and also present in the 3D porous Fe_3O_4/C composite flowers. In order to confirm this porous characteristic, the nitrogen adsorption–desorption isotherms and pore size distributions of the 3D porous Fe_3O_4/C composite flowers are displayed in Figure 5. The measured curves exhibit a similar IV-type isotherm with a long and narrow hysteresis loop at relative pressure from 0.4 to 1.0, implying the presence of mesopores in the 3D porous Fe_3O_4/C composite flowers.[25,26] Observing from the pore size distribution curve (inset of Figure 5), the pores size of ca. 25 nm takes the dominant position. The BET specific surface area of the 3D porous Fe_3O_4/C composite flowers are 70.2 m^2 g^{-1} is larger than that of Fe_3O_4/C nanorings (32.46 m^2 g^{-1}),[8]

DOI: 10.1021/acssuschemeng.8b03097
ACS Sustainable Chem. Eng. 2018, 6, 12471–12480

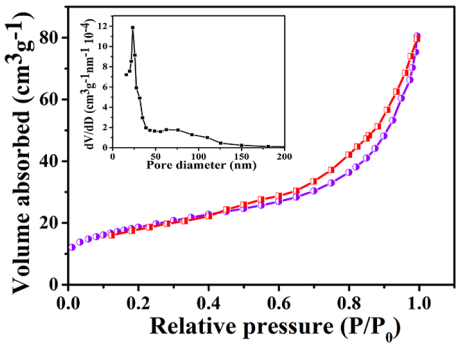

Figure 5. Nitrogen adsorption/desorption isotherms and inset is the corresponding pore size distribution curves of the 3D porous Fe_3O_4/C composite flowers.

porous Fe_3O_4/C nanorods (45.2 m^2 g^{-1}),[16] mesoporous interconnected C-encapsulated Fe_3O_4 (51.72 m^2 g^{-1}).[27]

Figure 6 shows the magnetic hysteresis loops of the 3D porous Fe_3O_4/C composite flowers. The saturation magnet-

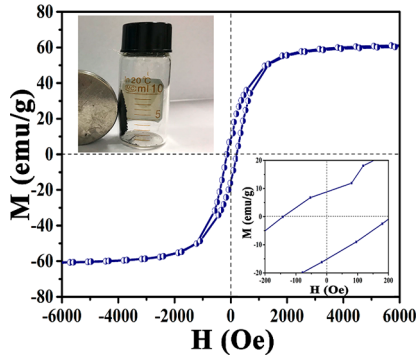

Figure 6. Magnetic hysteresis loop of the 3D porous Fe_3O_4/C composite flowers measured at room temperature. Inset of Figure 6 in the lower right-hand corner shows expanded low field hysteresis curves. Inset in the upper left-hand corner shows the rapid separation of 3D porous Fe_3O_4/C composite flowers by a magnet.

ization (M_s) value for the 3D porous Fe_3O_4/C composite flowers is 61.9 emu g^{-1}. As an indicator of the ferromagnetic property and high magnetization value, a rapid separation by a magnet has been observed in the upper left-handed corner of Figure 6. The M_s is lower than that of bulk Fe_3O_4 (92 emu g^{-1})[16] and the decreased M_s can be ascribed to the addition of nonmagnetic carbon. The coercive force (H_c) observed from the expanded low field hysteresis curves of inset Figure 6 shows that the 3D porous Fe_3O_4/C composite flowers own a large H_c value of 215.8 Oe. It is widely accepted that the H_c value is strongly related to particle size, shape and magneto-crystalline anisotropy.[28−30] In this study, the enhanced coercivity value is owing to the larger surface anisotropic energy induced by the large surface of 3D Fe_3O_4/C flowers.[19,31] Similar enhancement in H_c has been reported in many flower-like, or hierarchical structures.[18,19,32−34]

To reveal the EM wave absorption properties of the epoxy resin composites with 50 wt % 3D porous Fe_3O_4/C composite flowers, the RL was calculated from the measured complex permittivity and complex permeability at a given absorber thickness and frequency based on the transmit line theory, which can be expressed as follows:[35,36]

$$Z_{in} = Z_0(\mu_r/\varepsilon_r)^{1/2}\tanh\{j(2\pi fd/c)(\mu_r\varepsilon_r)^{1/2}\} \quad (2)$$

$$RL = 20\log|(Z_{in} - Z_0)/(Z_{in} + Z_0)| \quad (3)$$

where Z_0 refers to the input impedance of free space, Z_{in} is the input impedance of the absorber, f is the frequency, c is the velocity of light and d is the absorber thickness. In general, a RL value less than −10 dB (RL < −10 dB) is analogous to 90% EM absorption and the corresponding absorption frequency range with RL< −10 dB in one thickness is considered as effective bandwidth. Figure 7a shows the three-dimensional RL curves of the epoxy resin composites containing 50 wt % 3D porous Fe_3O_4/C composite flowers at various thicknesses over frequency range of 1−18 GHz. For an absorber thickness of 4.27 mm, the 3D porous Fe_3O_4/C composite flowers show an optimal RL value of −54.6 dB at 5.7 GHz, and the effective absorption bandwidth is 2.8 GHz (Figure 7b). When the thickness is decreased to 2.1 mm, the minimum RL value of −22.2 dB at 13.6 GHz is observed in Figure 7b and the achieved bandwidth with RL less than −10 dB is 6.0 GHz (12.0−18.0 GHz) as observed in Figure 7c. Besides, it can be found from Figure 7b that with a decrease in the thickness, the absorption peaks will shift to high frequency reigon. In order to explain this shift, the quarter-wavelength model $t_m = n\lambda/4 = nc/(4f_m\sqrt{|\mu_r||\varepsilon_r|})(n = 1, 3, 5...)$ are employed,[37] in which the absorber thickness (t_m) is inversely proportional to the peak frequency (f_m). Figure 7d presents the simulation of the absorber thickness versus peak frequency based on the quarter-wavelength ($\lambda/4$) condition. The red star in Figure 7d denotes the optimal thickness obtained directly from the 2D RL curves, Figure 7b. It is clear that all the red stars are located around the $t_m = \lambda/4$ curve, suggesting the relationship between matching thickness and frequency for the 3D porous Fe_3O_4/C composite flowers can be well-explained by the quarter-wavelength theory.

Compared with previously reported pure Fe_3O_4 absorber, the as-synthesized 3D porous Fe_3O_4/C composite flowers display great advantages, such as stronger absorption intensity, broader absorption bandwidth and thinner thickness. For example, the Fe_3O_4 nanoparticles,[38] Fe_3O_4 nanocrystals[39] and porous Fe_3O_4 flower-like nanostructures[21] exhibit a minimum RL value of −21.2, −21.1 and −28.3 dB, respectively, which is much lower than that of 3D porous Fe_3O_4/C composite flowers in this work (−54.6 dB). Such enhanced EM wave absorption performances of 3D porous Fe_3O_4/C composite flowers compared with pure Fe_3O_4 is ascribed to the improved impedance matching level resulted from an effective combination of dielectric loss from carbon and magnetic loss from Fe_3O_4 particles. For other reported Fe_3O_4/C composite absorbers, such as Fe_3O_4/C core−shell composites,[15] RGO-Fe_3O_4 composites,[41] Fe_3O_4/carbon core/shell nanorods,[16] the 3D porous Fe_3O_4/C composite flowers also show stronger absorption capacity and broader absorption bandwidth. The detailed comparations between the 3D porous Fe_3O_4/C composite flowers in this work and previously reported pure Fe_3O_4 absorber and other Fe_3O_4/C composites are listed in Table 1. Summarizing the comparative results in Table 1, the as-synthesized 3D porous Fe_3O_4/C composite flowers can be considered as an ideal absorption material with strong absorption ability, broad absorption bandwidth and thin absorber thickness.

In order to explore the intrinsic mechanisms for such excellent microwave absorption performances of the 3D

DOI: 10.1021/acssuschemeng.8b03097
ACS Sustainable Chem. Eng. 2018, 6, 12471−12480

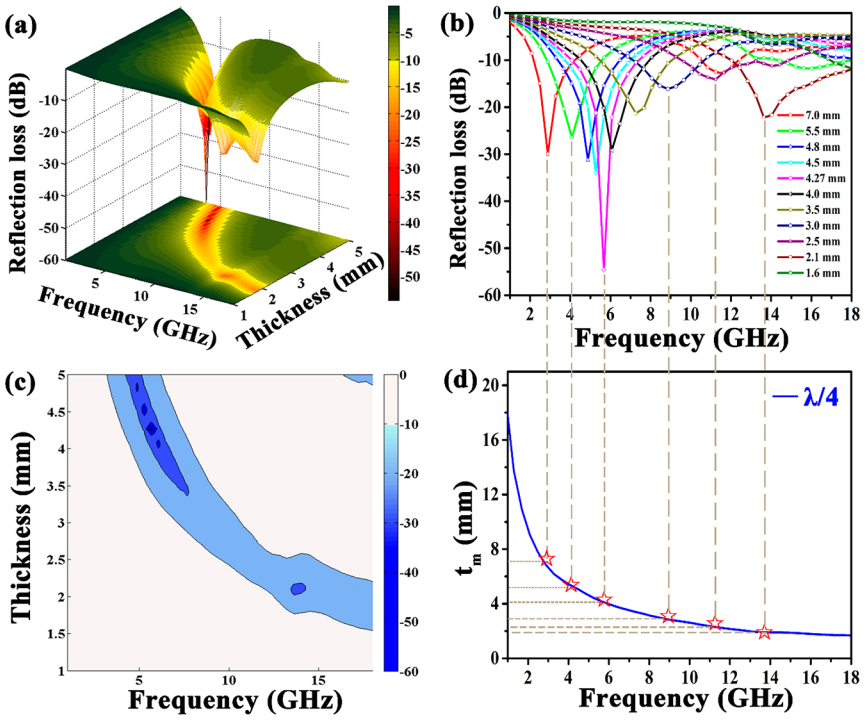

Figure 7. (a) 3D representations of calculated RL values, (b) frequency dependence of RL curves. (c) 2D contour plots of 3D RL representations and (d) simulations of the absorber thickness (t_m) versus peak frequency (f_m) for 3D porous Fe_3O_4/C composite flowers.

Table 1. EM Wave Absorption Properties of Previously Reported Pure Fe_3O_4 Absorber and Other Fe_3O_4/C Composites

Sample	Filling ratio	Optimal RL (dB)	Optimal Thickness (mm)	Bandwidth		ref
				Thickness (mm)	RL<-10 dB (GHz)	
Fe_3O_4 nanoparticles	60 wt %	−21.2	2.0	2.0	3.6 (14.4−18.0)	38
Fe_3O_4 nanocrystals	30 vol%	−21.1	5.0	2.0	–	39
porous Fe_3O_4 flower-like nanostructures	50 wt %	−28.3	2.0	2.0	3.8 (11.7−15.5)	21
Fe_3O_4/C nanospindles	60 wt %	−36.5	5.0	2.0	2.3 (10.5−12.8)	7
core−shell Fe_3O_4/C composites	50 wt %	−36.5	5.0	2.0	3.7 (11.8−15.5)	15
Fe_3O_4/carbon core/shell nanorods	55 wt %	−27.9	2.0	2.0	5.0 (13.0−18.0)	16
Fe_3O_4@C nanotubes	66.7 wt %	−22.6	1.7	2.0	4.8 (11.4−16.2)	40
RGO-Fe_3O_4 composites	40 wt %	−26.4	4.0	2.0	2.8 (10.4−13.2)	41
MWCNT/Fe_3O_4 hybrid materials	70 wt %	−18.2	2.0	2.0	–	42
3D porous Fe_3O_4/C composite flowers	50 wt %	−54.6	4.27	**2.1**	6.0 (12.0−18.0)	This work

porous Fe_3O_4/C composite flowers, the electromagnetic parameters including complex permittivity ($\varepsilon_r = \varepsilon' - j\varepsilon''$) and complex permeability ($\mu_r = \mu' - j\mu''$) were investigated, where the real parts (ε' and μ') and imaginary parts (ε'' and μ'') stand for the storage and loss capability of electric and magnetic energy, respectively. As displayed in Figure 8a, the ε' values tend to decrease continuously with negligible fluctuations from 9.51 to 5.32 while ε'' decreases gradually from the maximum value of 2.65 at 13.8 GHz for 3D porous Fe_3O_4/C composite flowers with the increasing frequency. Meanwhile, a distinguishable peak was observed in the ε'' curves at 13.8 GHz is associated with a dielectric polarization behavior (e.g., ionic polarization, electric polarization, dipolar polarization, interface polarization etc.).[12,37] As ionic polarization, and electron polarization generally exist in much higher frequency region (10^3−10^6 GHz), which could be easily excluded easily.[43] To clarify the reasons for the presence of the resonance peak in ε'' curves and understand the dielectric loss mechanisms of 3D porous Fe_3O_4/C composite flowers, the Debye dipolar relaxation model was employed.[8] According to the Debye dipolar relaxation, the complex permittivity can be described as equation 4:[44]

$$\varepsilon_r = \varepsilon' - j\varepsilon'' = \varepsilon_\infty + (\varepsilon_s - \varepsilon_\infty)/(1 + j\omega\tau) \quad (4)$$

in which ω ($\omega = 2\pi f$), ε_s, τ and ε_∞ represent the angular frequency, static permittivity, relaxation time and relative permittivity at the high-frequency limit. Based on the above equation 4, ε' and ε'' could be deduced that

$$\varepsilon' = \varepsilon_\infty + (\varepsilon_s - \varepsilon_\infty)/(1 + \omega^2\tau^2) \quad (5)$$

$$\varepsilon'' = \omega\tau + (\varepsilon_s - \varepsilon_\infty)/(1 + \omega^2\tau^2) \quad (6)$$

The continuous decrease for the ε' curve in Figure 8a with frequency can be well explained by using Equation 5, in which the ε' value is inversely proportional to frequency. According to Equations 5 and 6, the relationship between ε' and ε'' can be expressed as

DOI: 10.1021/acssuschemeng.8b03097
ACS Sustainable Chem. Eng. 2018, 6, 12471−12480

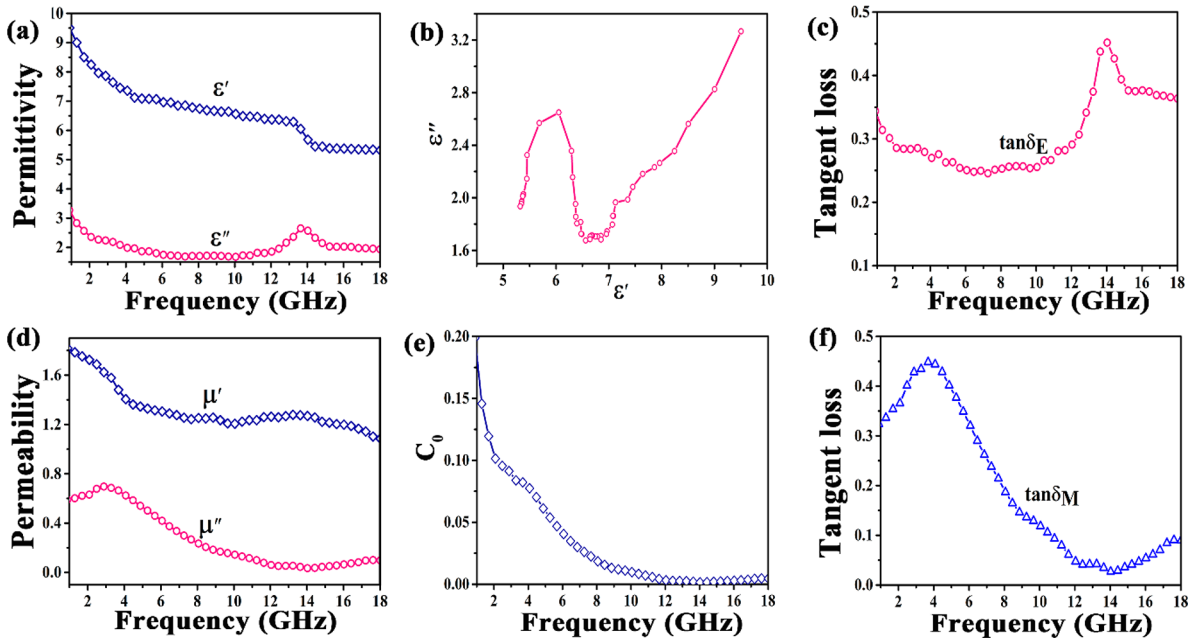

Figure 8. Frequency dependence of (a) complex permittivity, (c) dielectric tangent loss, (d) complex permeability, (e) C_0 values (representing eddy current loss), (f) magnetic tangent loss for 3D porous Fe_3O_4/C composite flowers. (b) Cole−Cole semicircles (ε' versus ε'').

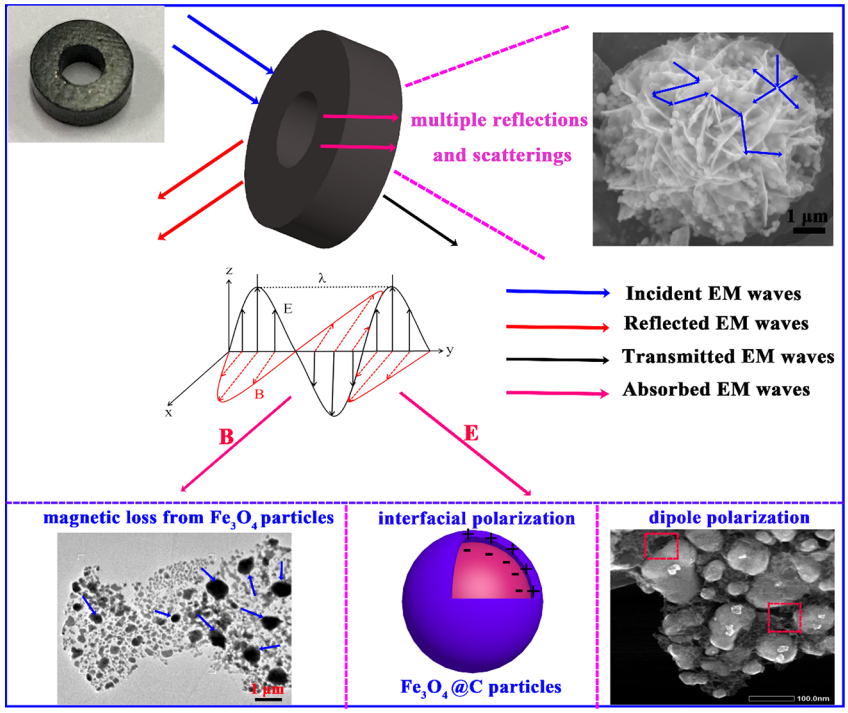

Figure 9. Schematic illustration of the EM wave absorption mechanisms for 3D porous Fe_3O_4/C composite flowers.

$$[\varepsilon' - (\varepsilon_s + \varepsilon_\infty)/2]^2 + (\varepsilon'')^2 = [(\varepsilon_s - \varepsilon_\infty)/2]^2 \quad (7)$$

If ε' and ε'' of an absorber satisfy Equation 7, the plot of ε' against ε'' should be a single semicircle, known as the Cole−Cole semicircle, corresponding to one Debye dipolar relaxation.[3,45] Figure 8b shows the curves of ε' plotted against ε'' for 3D porous Fe_3O_4/C composite flowers, in which one semicircle was present, demonstrating the existence of Debye dipolar relaxation process. For the as-synthesized 3D porous Fe_3O_4/C composite flowers, the Debye dipolar relaxation process mainly originates from the following aspects. The first is the interfacial polarization, which exists in the interface between Fe_3O_4 core and carbon shell. Owing to the presence of heterogeneous interfaces, the charges will accumulate at the interfaces and produce an electric dipole moment, which results in interfacial relaxation.[45,46] Second, the abundant defects existed on the surface of carbon shell and carbon sheet can act as polarization centers, which will generate polarization relaxation under the electromagnetic field.[47,48] Figure 8d shows the frequency dependence of complex permeability for the epoxy resin composites containing 50 wt % 3D porous Fe_3O_4/C composite flowers. As observed, the μ' values decrease from

DOI: 10.1021/acssuschemeng.8b03097
ACS Sustainable Chem. Eng. 2018, 6, 12471−12480

1.82 to 1.08 over 1−18 GHz while μ'' exhibits two resonance peaks between 2.0 and 8.0 GHz and 14.0−18.0 GHz, respectively. Generally, the magnetic loss often occurs from the relaxation process during magnetization, which mainly consists of domain wall resonance, exchange resonance, eddy current and natural resonance.[49] As the domain wall resonance usually occurs in the low frequency range (<2 GHz), which can be excluded first.[49] The eddy current loss is related to the thickness (d) and electric conductivity (σ) of the materials, which can be expressed by[49,50]

$$C_0 = \mu''(\mu')^{-2}f^{-1} = 2\pi\mu_0 d^2\sigma \quad (8)$$

Supposing that the magnetic loss totally originates from eddy current loss, then the value of C_0 should be constant when frequency varies. It can be seen from Figure 8e that the C_0 varies with increasing frequency, indicating that the eddy current can be suppressed effectively and the eddy current loss is not the main origin of magnetic loss. Concluded from the above analysis, the natural resonance and exchange resonance should be the dominant magnetic loss mechanisms for 3D porous Fe_3O_4/C composite flowers. According to reports, the resonance peaks of μ'' at low frequency from 2.0 to 8.0 GHz should belong to natural resonance while the high frequency resonance peaks from 14.0 to 18.0 GHz can be attributed to exchange resonance.[49]

It is widely known that the dielectric loss and magnetic loss are two key attenuation mechanisms for EM wave absorption. In order to determine which one is dominating for the 3D porous Fe_3O_4/C composite flowers, the dielectric loss tangent and magnetic loss tangent are calculated and displayed in Figure 8c,f. From 1.0 to 8.0 GHz, the tan δ_M (0.32−0.46) is close to tan δ_E (0.25−0.35), inferring that both magnetic loss and dielectric loss contributes to EM wave absorption in this frequency region. From 8.0 to 18.0 GHz, the tan δ_M values decrease rapidly while the tan δ_E curve shows an increasing trend, which suggests that dielectric loss is the main mechanism for EM absorption rather than magnetic loss in the high frequency range. The dielectric loss as the dominant mechanism at high frequency range has been reported in various kinds of magnetic carbon composites, such as Fe_3O_4@C core−shell nanotubes,[40] RGo-Fe_3O_4 composite,[41] Fe/C nanocubes[51] and GO/CNT-Fe_3O_4 composites.[52]

Based on the above analysis, the enhanced EM wave absorption performances of the 3D porous Fe_3O_4/C composite flowers can be understood by the following aspects shown in Figure 9. First, owing to the synergistic effect of magnetic loss from Fe_3O_4 and dielectric loss from carbon, a good impedance matching can be obtained (shown in Figure 8c,f), endowing the 3D porous Fe_3O_4/C composite flowers with enhanced EM wave absorption properties. The dipolar polarization and interfacial polarization are the main causes of dielectric loss while the magnetic loss mainly originates from natural resonance and exchange resonance. Finally, the 3D porous Fe_3O_4/C composite flowers with large surface area promote the production of multiple reflections, which prolongs the travel path and attenuates the incident wave energy gradually.[10,53] The porous structure is beneficial to modify the permittivity and improve the impedance matching level. According to the Maxwell−Garnett (MG) theory, which is shown as below:[35]

$$\varepsilon_{\text{eff}}^{\text{MG}} = \varepsilon_1 \frac{(\varepsilon_2 + 2\varepsilon_1) + 2p(\varepsilon_2 - \varepsilon_1)}{(\varepsilon_2 + 2\varepsilon_1) - p(\varepsilon_2 - \varepsilon_1)} \quad (9)$$

where ε_1 and ε_2 represent the dielectric constant of the host (solid) and guest (air), p is the volume fraction of guest in the porous materials. As the ε_1 value is much larger than ε_2 ($\varepsilon_2 \approx 1$), with the increase of pore volume, p will increase which leads to the decrease of effective permittivity. In this way, the permittivity of the porous Fe_3O_4/C composite flowers can be tuned. Besides, the pores and defects present on the amorphous carbon sheet and carbon shell of 3D porous Fe_3O_4/C composite flowers serve as scattering centers, providing another mechanism for EM wave attenuation.[54,55] In conclusion, the as-synthesized 3D porous Fe_3O_4/C composite flowers can be considered as an ideal absorber with strong absorption capacity, thin absorber thickness and broad bandwidth. Besides, owing to wide applications of magnetic carbon materials,[56−59] the 3D porous Fe_3O_4/C composite flowers can be further extended to other fields.

CONCLUSIONS

3D porous Fe_3O_4/C composite flowers were successfully prepared through a facile strategy including a solvothermal approach and a following carbon reduction process. The epoxy resin composites containing 50 wt % 3D porous Fe_3O_4/C composite flowers exhibit an enhanced EM wave absorption comparing with previously reported pure Fe_3O_4 and other Fe_3O_4/C composites. The improved EM wave absorption of the 3D porous Fe_3O_4/C composite flowers are interpreted from the improved impedance matching resulting from an effective combination of strong magnetic loss from Fe_3O_4 and dielectric loss from carbon, as well as the multiple reflections and scatterings arising from the three-dimensional and porous structural advantages. Besides, the core−shell structure significantly improves the antioxidant ability of Fe_3O_4 particles. This work suggests the 3D porous Fe_3O_4/C composite flowers can be regarded as a potential candidate for enhanced EM wave absorption.

AUTHOR INFORMATION

Corresponding Author

*E-mail: jrliu@sdu.edu.cn (J. Liu).

ORCID

Wei Liu: 0000-0002-8653-8228

Zhanhu Guo: 0000-0003-0134-0210

Notes

The authors declare no competing financial interest.

ACKNOWLEDGMENTS

This work was supported by the National Natural Science Foundation of China (No. 51572157) and the Natural Science Foundation of Shandong Province (ZR2016BM16) and China Scholar Council.

REFERENCES

(1) Xie, P.; Li, H.; He, B.; Dang, F.; Lin, J.; Fan, R.; Hou, C.; Liu, H.; Zhang, J.; Ma, Y.; Guo, Z. Bio-gel derived nickel/carbon nanocomposites with enhanced microwave absorption. *J. Mater. Chem. C* **2018**, *6*, 8812−8822.

(2) Wu, N.; Qiao, J.; Liu, J.; Du, W.; Xu, D.; Liu, W. Strengthened electromagnetic absorption performance derived from synergistic

DOI: 10.1021/acssuschemeng.8b03097
ACS Sustainable Chem. Eng. 2018, 6, 12471−12480

effect of carbon nanotube hybrid with Co@C beads. *Adv. Compos. Hybrid Mater.* **2018**, *1*, 149−159.
(3) Kong, L.; Yin, X.; Yuan, X.; Zhang, Y.; Liu, X.; Cheng, L.; Zhang, L. Electromagnetic wave absorption properties of graphene modified with carbon nanotube/poly(dimethyl siloxane) composites. *Carbon* **2014**, *73*, 185−193.
(4) Lv, L.; Liu, J.; Liu, H.; Liu, C.; Lu, Y.; Sun, K.; Fan, R.; Wang, N.; Lu, N.; Guo, Z.; Wujcik, E. An overview of electrically conductive polymer nanocomposites toward electromagnetic interference shielding. *Eng. Sci.* **2018**, *2*, 26−42.
(5) Zhao, B.; Deng, J.; Zhang, R.; Liang, L.; Fan, B.; Bai, Z.; Shao, G.; Park, C. B. Recent advances on the electromagnetic wave absorption properties of Ni based materials. *Eng. Sci.* **2018**, DOI: 10.30919/es8d735.
(6) Zhang, K.; Li, G.; Feng, L.; Wang, N.; Guo, J.; Sun, K.; Yu, K.; Zeng, J.; Li, T.; Guo, Z.; Wang, M. Ultralow percolation threshold and enhanced electromagnetic interference shielding in poly(L-lactide)/multi-walled carbon nanotube nanocomposites with electrically conductive segregated networks. *J. Mater. Chem. C* **2017**, *5*, 9359−9369.
(7) Liu, X.; Cui, X.; Chen, Y.; Zhang, X.; Yu, R.; Wang, G.; Ma, H. Modulation of electromagnetic wave absorption by carbon shell thickness in carbon encapsulated magnetite nanospindlese-poly-(vinylidene fluoride) composites. *Carbon* **2015**, *95*, 870−878.
(8) Wu, T.; Liu, Y.; Zeng, X.; Cui, T.; Zhao, Y.; Li, Y.; Tong, G. Facile hydrothermal synthesis of Fe_3O_4/C core-shell nanorings for efficient low-frequency microwave absorption. *ACS Appl. Mater. Interfaces* **2016**, *8*, 7370−7380.
(9) Xu, J.; Liu, J.; Che, R.; Liang, C.; Cao, M.; Li, Y.; Liu, Z. Polarization enhancement of microwave absorption by increasing aspect ratio of ellipsoidal nanorattles with Fe_3O_4 cores and hierarchical $CuSiO_3$ shells. *Nanoscale* **2014**, *6*, 5782−5790.
(10) Liang, C.; Liu, C.; Wang, H.; Wu, L.; Jiang, Z.; Xu, Y.; Shen, B.; Wang, Z. SiC−Fe_3O_4 dielectric−magnetic hybrid nanowires: controllable fabrication, characterization and electromagnetic wave absorption. *J. Mater. Chem. A* **2014**, *2*, 16397−16402.
(11) Wang, F.; Liu, J.; Kong, J.; Zhang, Z.; Wang, X.; Itoh, M.; Machida, K. Template free synthesis and electromagnetic wave absorption properties of monodispersed hollow magnetite nanospheres. *J. Mater. Chem.* **2011**, *21*, 4314−4320.
(12) Xiang, J.; Li, J.; Zhang, X.; Ye, Q.; Xu, J.; Shen, X. Magnetic carbon nanofibers containing uniformly dispersed Fe/Co/Ni nanoparticles as stable and high-performance electromagnetic wave absorbers. *J. Mater. Chem. A* **2014**, *2*, 16905−16914.
(13) Lü, Y.; Wang, Y.; Li, H.; Lin, Y.; Jiang, Z.; Xie, Z.; Kuang, Q.; Zheng, L. MOF-derived porous Co/C nanocomposites with excellent electromagnetic wave absorption properties. *ACS Appl. Mater. Interfaces* **2015**, *7*, 13604−13611.
(14) Li, X.; Feng, J.; Du, Y.; Bai, J.; Fan, H.; Zhang, H.; Peng, Y.; Li, F. One-pot synthesis of $CoFe_2O_4$/graphene oxide hybrids and their conversion into FeCo/graphene hybrids for lightweight and highly efficient microwave absorber. *J. Mater. Chem. A* **2015**, *3*, 5535−5546.
(15) Du, Y.; Liu, W.; Qiang, R.; Wang, Y.; Han, X.; Ma, J.; Xu, P. Shell thickness-dependent microwave absorption of core−shell Fe_3O_4@C composites. *ACS Appl. Mater. Interfaces* **2014**, *6*, 12997−13006.
(16) Chen, Y.-J.; Xiao, G.; Wang, T.-S.; Ouyang, Q.-Y.; Qi, L.-H.; Ma, Y.; Gao, P.; Zhu, C.-L.; Cao, M.-S.; Jin, H.-B. Porous Fe_3O_4/carbon core/shell nanorods: synthesis and electromagnetic properties. *J. Phys. Chem. C* **2011**, *115*, 13603−13608.
(17) Wang, C.; Han, X.; Xu, P.; Wang, J.; Du, Y.; Wang, X.; Qin, W.; Zhang, T. Controlled synthesis of hierarchical nickel and morphology-dependent electromagnetic properties. *J. Phys. Chem. C* **2010**, *114*, 3196−3203.
(18) Lv, H.; Liang, X.; Ji, G.; Zhang, H.; Du, Y. Porous three-dimensional flower-like Co/CoO and its excellent electromagnetic absorption properties. *ACS Appl. Mater. Interfaces* **2015**, *7*, 9776−9783.
(19) Wang, X.; Shi, G.; Shi, F.-N.; Xu, G.; Qi, Y.; Li, D.; Zhang, Z.; Zhang, Y.; You, H. Synthesis of hierarchical cobalt dendrites based on nanoflake self-assembly and their microwave absorption properties. *RSC Adv.* **2016**, *6*, 40844−40853.
(20) Feng, C.; Liu, X.; Sun, Y.; Jin, C.; Lv, Y. Enhanced microwave absorption of flower-like FeNi@C nanocomposites by dual dielectric relaxation and multiple magnetic resonance. *RSC Adv.* **2014**, *4*, 22710−22715.
(21) Li, X.; Zhang, B.; Ju, C.; Han, X.; Du, Y.; Xu, P. Morphology-controlled synthesis and electromagnetic properties of porous Fe_3O_4 nanostructures from iron alkoxide precursors. *J. Phys. Chem. C* **2011**, *115*, 12350−12357.
(22) Zhao, Z.; Bai, P.; Guan, R.; Murugadoss, V.; Liu, H.; Wang, X.; Guo, Z. Microstructural evolution and mechanical strengthening mechanism of Mg-3Sn-1Mn-1La alloy after heat treatments. *Mater. Sci. Eng., A* **2018**, *734*, 200.
(23) Zhao, Z.; Guan, R.; Zhang, J.; Zhao, Z.; Bai, P. Effects of process parameters of semisolid stirring on microstructure of Mg−3Sn−1Mn−3SiC (wt%) strip processed by rheo-rolling. *Acta Metall. Sin. (Engl. Lett.)* **2017**, *30*, 66−72.
(24) Guo, S.; Liu, J.; Qiu, S.; Liu, W.; Wang, Y.; Wu, N.; Guo, J.; Guo, Z. Porous ternary TiO_2/$MnTiO_3$@C hybrid microspheres as anode materials with enhanced electrochemical performances. *J. Mater. Chem. A* **2015**, *3*, 23895−23904.
(25) Liu, W.; Shao, G.; Ji, G.; Liang, X.; Cheng, Y.; Quan, B.; Du, Y. Metal−organic-frameworks derived porous carbon-wrapped Ni composites with optimized impedance matching as excellent lightweight electromagnetic wave absorber. *Chem. Eng. J.* **2017**, *313*, 734−744.
(26) Guo, S.; Lu, G.; Qiu, S.; Liu, J.; Wang, X.; He, C.; Wei, H.; Yan, X.; Guo, Z. Carbon-coated MnO microparticulate porous nanocomposites serving as anode materials with enhanced electrochemical performances. *Nano Energy* **2014**, *9*, 41−49.
(27) Liu, J.; Zhou, Y.; Liu, F.; Liu, C.; Wang, J.; Pan, Y.; Xue, D. One-pot synthesis of mesoporous interconnected carbon-encapsulated Fe_3O_4 nanospheres as superior anodes for Li-Ion batteries. *RSC Adv.* **2012**, *2*, 2262−2265.
(28) Lv, H.; Liang, X.; Cheng, Y.; Zhang, H.; Tang, D.; Zhang, B.; Ji, G.; Du, Y. Coin-like α-Fe_2O_3@$CoFe_2O_4$ core−shell composites with excellent electromagnetic absorption performance. *ACS Appl. Mater. Interfaces* **2015**, *7*, 4744−4750.
(29) Jiang, L.; Wang, Z.; Li, D.; Geng, D.; Wang, Y.; An, J.; He, J.; Liu, W.; Zhang, Z. Excellent microwave-absorption performances by matched magnetic−dielectric properties in double-shelled Co/C/polyaniline nanocomposites. *RSC Adv.* **2015**, *5*, 40384−40392.
(30) Zhang, S.; Jiao, Q.; Zhao, Y.; Li, H.; Wu, Q. Preparation of rugby-shaped $CoFe_2O_4$ particles and their microwave absorbing properties. *J. Mater. Chem. A* **2014**, *2*, 18033−18039.
(31) He, C.; Qiu, S.; Wang, X.; Liu, J.; Luan, L.; Liu, W.; Itoh, M.; Machida, K. Facile synthesis of hollow porous cobalt spheres and their enhanced electromagnetic properties. *J. Mater. Chem.* **2012**, *22*, 22160−22166.
(32) Liu, Q.; Xu, X.; Xia, W.; Che, R.; Chen, C.; Cao, Q.; He, J. Dependency of magnetic microwave absorption on surface architecture of $Co_{20}Ni_{80}$ hierarchical structures studied by electron holography. *Nanoscale* **2015**, *7*, 1736−1743.
(33) Gao, S.; Zhou, N.; An, Q.; Xiao, Z.; Zhai, S.; Shi, Z. Facile solvothermal synthesis of novel hetero-structured CoNi−CuO composites with excellent microwave absorption performance. *RSC Adv.* **2017**, *7*, 43689−43699.
(34) Wei, S.; Wang, X.; Zhang, B.; Yu, M.; Zheng, Y.; Wang, Y.; Liu, J. Preparation of hierarchical core-shell C@$NiCo_2O_4$@Fe_3O_4 composites for enhanced microwave absorption performance. *Chem. Eng. J.* **2017**, *314*, 477−487.
(35) Quan, B.; Liang, X.; Ji, G.; Zhang, Y.; Xu, G.; Du, Y. Cross-linking-derived synthesis of porous Co_xNi_y/C nanocomposites for excellent electromagnetic behaviors. *ACS Appl. Mater. Interfaces* **2017**, *9*, 38814−38823.

(36) Liu, J. R.; Itoh, M.; Machida, K. Magnetic and electromagnetic wave absorption properties of α-Fe/Z-Type Ba-Ferrite nanocomposites. *Appl. Phys. Lett.* **2006**, *88*, 062503.
(37) Yin, Y.; Liu, X.; Wei, X.; Li, Y.; Nie, X.; Yu, R.; Shui, J. Magnetically aligned Co-C/MWCNTs composite derived from MWCNT-interconnected zeolitic imidazolate frameworks for a lightweight and highly efficient electromagnetic wave absorber. *ACS Appl. Mater. Interfaces* **2017**, *9*, 30850−30861.
(38) Wang, G.; Chang, Y.; Wang, L.; Liu, L.; Liu, C. Facilely preparation and microwave absorption properties of Fe_3O_4 nanoparticles. *Mater. Res. Bull.* **2013**, *48*, 1007−1012.
(39) Ni, S.; Lin, S.; Pan, Q.; Yang, F.; Huang, K.; He, D. Hydrothermal synthesis and microwave absorption properties of Fe_3O_4 nanocrystals. *J. Phys. D: Appl. Phys.* **2009**, *42*, 055004.
(40) Li, W.; Lv, B.; Wang, L.; Li, G.; Xu, Y. Fabrication of Fe_3O_4@C core−shell nanotubes and their application as a lightweight microwave absorbent. *RSC Adv.* **2014**, *4*, 55738−55744.
(41) Sun, X.; He, J.; Li, G.; Tang, J.; Wang, T.; Guo, Y.; Xue, H. Laminated magnetic graphene with enhanced electromagnetic wave absorption properties. *J. Mater. Chem. C* **2013**, *1*, 765−777.
(42) Hou, C.; Li, T.; Zhao, T.; Liu, H.; Liu, L.; Zhang, W. Electromagnetic wave absorbing properties of multi-wall carbon nanotube/Fe_3O_4 hybrid materials. *New Carbon Mater.* **2013**, *28*, 184−190.
(43) Asami, K. Characterization of heterogeneous systems by dielectric spectroscopy. *Prog. Polym. Sci.* **2002**, *27*, 1617−1659.
(44) Qi, X.; Hu, Q.; Cai, H.; Xie, R.; Bai, Z.; Jiang, Y.; Qin, S.; Zhong, W.; Du, Y. Hetero-nanostructured Co@carbon nanotubes-graphene ternary hybrids: synthesis, electromagnetic and excellent microwave absorption properties. *Sci. Rep.* **2016**, *6*, 1−15.
(45) Liu, X. G.; Jiang, J. J.; Geng, D. Y.; Li, B. Q.; Han, Z.; Liu, W.; Zhang, Z. D. Dual nonlinear dielectric resonance and strong natural resonance in Ni/ZnO nanocapsules. *Appl. Phys. Lett.* **2009**, *94*, 053119.
(46) Liu, T.; Xie, X.; Pang, Y.; Kobayashi, S. Co/C nanoparticles with low graphitization degree: a high performance microwave-absorbing material. *J. Mater. Chem. C* **2016**, *4*, 1727−1735.
(47) Wang, H.; Xiang, L.; Wei, W.; An, J.; He, J.; Gong, C.; Hou, Y. Efficient and lightweight electromagnetic wave absorber derived from metal organic framework-encapsulated cobalt nanoparticles. *ACS Appl. Mater. Interfaces* **2017**, *9*, 42102−42110.
(48) Watts, P. C. P.; Hsu, W.-K.; Barnes, A.; Chambers, B. High permittivity from defective multiwalled carbon nanotubes in the X-band. *Adv. Mater.* **2003**, *15*, 600−603.
(49) Zhao, B.; Guo, X.; Zhao, W.; Deng, J.; Shao, G.; Fan, B.; Bai, Z.; Zhang, R. Yolk−shell Ni@SnO_2 composites with a designable interspace to improve the electromagnetic wave absorption properties. *ACS Appl. Mater. Interfaces* **2016**, *8*, 28917−28925.
(50) Wu, M.; Zhang, Y. D.; Hui, S.; Xiao, T. D.; Ge, S.; Hines, W. A.; Budnick, J. I.; Taylor, G. W. Microwave magnetic properties of $Co_{50}/(SiO_2)_{50}$ nanoparticles. *Appl. Phys. Lett.* **2002**, *80*, 4404−4406.
(51) Qiang, R.; Du, Y.; Zhao, H.; Wang, Y.; Tian, C.; Li, Z.; Han, X.; Xu, P. Metal organic framework-derived Fe/C nanocubes toward efficient microwave absorption. *J. Mater. Chem. A* **2015**, *3*, 13426−13434.
(52) Wang, L.; Jia, X.; Li, Y.; Yang, F.; Zhang, L.; Liu, L.; Ren, X.; Yang, H. Synthesis and microwave absorption property of flexible magnetic film based on graphene oxide/carbon nanotubes and Fe_3O_4 nanoparticles. *J. Mater. Chem. A* **2014**, *2*, 14940−14946.
(53) Fang, J.; Liu, T.; Chen, Z.; Wang, Y.; Wei, W.; Yue, X.; Jiang, Z. A wormhole-like porous carbon/magnetic particles composite as an efficient broadband electromagnetic wave absorber. *Nanoscale* **2016**, *8*, 8899−8909.
(54) Knoch, D.; Pascual-Leone, A.; Meyer, K.; Treyer, V.; Fehr, E. Diminishing reciprocal fairness by disrupting the right prefrontal cortex. *Science* **2006**, *314*, 829−832.
(55) Sun, S.; He, Q.; Xiao, S.; Xu, Q.; Li, X.; Zhou, L. Gradient-index meta-surfaces as a bridge linking propagating waves and surface waves. *Nat. Mater.* **2012**, *11*, 426−431.
(56) Zhang, Y.; Qian, L.; Zhao, W.; Li, X.; Huang, X.; Mai, Z.; Wang, Z.; Shao, Q.; Yan, X.; Guo, Z. Highly efficient Fe-N-C nanoparticles modified porous graphene composites for oxygen reduction reaction. *J. Electrochem. Soc.* **2018**, *165*, H510−H516.
(57) Li, Y.; Jing, T.; Xu, G.; Tian, J.; Dong, M.; Shao, Q.; Wang, B.; Wang, Z.; Zheng, Y.; Yang, C.; Guo, Z. 3-D magnetic graphene oxide-magnetite poly(vinyl alcohol) nanocomposite substrates for immobilizing enzyme. *Polymer* **2018**, *149*, 13−22.
(58) Huang, J.; Cao, Y.; Shao, Q.; Peng, X.; Guo, Z. Magnetic nanocarbon adsorbents with enhanced hexavalent chromium removal: morphology dependence of fibrillar vs particulate structures. *Ind. Eng. Chem. Res.* **2017**, *56*, 10689−10701.
(59) Huang, J.; Li, Y.; Cao, Y.; Peng, F.; Cao, Y.; Shao, Q.; Liu, H.; Guo, Z. Hexavalent chromium removal over magnetic carbon nanoadsorbent: synergistic effect of fluorine and nitrogen Co-doping. *J. Mater. Chem. A* **2018**, *6*, 13062−13074.

DOI: 10.1021/acssuschemeng.8b03097
ACS Sustainable Chem. Eng. 2018, 6, 12471−12480